Understanding multidecadal variability in ENSO amplitude

ALEXANDRIA M. RUSSELL and ANAND GNANADESIKAN

Johns Hopkins University, Earth and Planetary Sciences Department

ABSTRACT

Sea surface temperatures (SSTs) in the tropical Pacific vary as a result of the coupling between the ocean and atmosphere driven largely by the El Niño – Southern Oscillation (ENSO). ENSO has a large impact on the local climate and hydrology of the tropical Pacific, as well as broad-reaching effects on global climate. ENSO is known to vary on long timescales (Wittenberg 2009), which makes it very difficult to quantify its response to climate change and constrain the physical processes that drive it. In order to assess the long-term changes in ENSO variability, a linear regression of SST changes based on van Oldenborgh et al. (2005) is applied to the GFDL CM2.1 model 4000-yr pre-industrial control run. The resulting parameter strengths, which represent the sensitivity of SST changes to thermocline depth and zonal wind stress, vary by up to a factor of 2 on multi-decadal time scales. This long-term modulation in ocean-atmosphere coupling is highly correlated with ENSO variability. Variation in the relationship between SST changes and wind stress points to a role for changing stratification in the central equatorial Pacific in modulating ENSO amplitudes. In addition, there is a higher ENSO variance during decades when the thermocline is flatter and when the zonal winds are more responsive. This indirect relationship between thermocline depth and atmospheric response appears to account for the relationship between the associated regression coefficients and ENSO variance. These mechanisms drive much of the variability in ENSO amplitude and hence ocean-atmosphere coupling in the tropical Pacific.

1. Introduction

El Niño – Southern Oscillation (ENSO) accounts for most of the interannual variability in global temperature and has links to global hydrological cycling and weather patterns. Therefore, it is important to understand how the amplitude of ENSO varies with time. It is unclear what length of time is adequate to constrain ENSO variability and what causes this long time-period variation. In evaluating a 2000-yr control simulation of the GFDL CM2.1 coupled GCM with

constant 1860 values for atmospheric composition, solar irradiance and land cover, Wittenberg (2009) determined that ENSO amplitude varies on centennial scales. He found that centennial spectra have extremes spanning a factor of 2 in power in the interannual band, with an even larger spread of spectra for 20-yr epochs. He hypothesized that this slow variation of ENSO results from Poisson statistical behavior due to seasonal phase-locking and interannual memory on scales of up to 10 years. This implies that the variation in ENSO amplitude may be largely random on long timescales, which would lead one to expect the coupling between the ocean and the atmosphere to be constant in a control simulation.

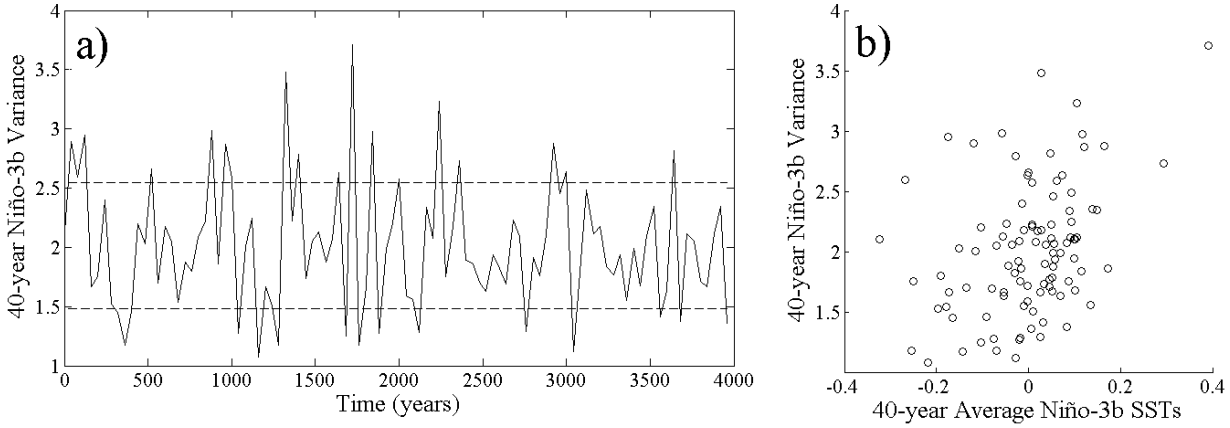

Figure 1. (a) 40-yr variance of Niño-3b SST anomalies from the GDFL CM2.1 4000-yr control simulation where the dashed lines mark the mean +/- the standard deviation (b) the 40-yr variance vs. the 40-yr average of Niño-3b SST anomalies.

In this paper, we examine an extended version of the model dataset studied by Wittenberg (2009). In the 4000-yr GFDL CM2.1 1860 control run the variance in the Niño-3b region (150W-90W, 3S-3N) ranges over a factor of 3 between different 40-yr epochs (Fig. 1a). Such long period variability has consequences for evaluating and using climate models. For instance, it may require multiple centuries to capture the full range of ENSO amplitude variability in climate models. It follows that it would also require multi-century model runs to detect changes in the normal ENSO behavior due to anthropogenic forcings. Stevenson et al. (2012) evaluated

CCSM4 Coupled Model Intercomparison Project phase 5 (CMIP5) simulations and found that there are no statistically significant changes to ENSO variability with increases in CO_2, except at the highest CO_2 levels. They postulated that this lack of significance is due to the short length of the twenty-first-century simulations. This supports Wittenberg (2009) in that it would require a longer timescale to distinguish relatively small ENSO amplitude responses to CO_2-based climate change from normal multidecadal variability.

This paper investigates the intrinsic non-climate-forced ENSO variability on multidecadal time scales. One possibility is that these changes in variance are the result of variability in the mean tropical temperatures. If true, this might have important implications for understanding the response to climate change. However, it is evident that the mean temperature is not a very good predictor of overall variance. The standard deviation of the 40-yr average Niño-3b SSTs is only about 0.1 °C, while the range is about 0.7 °C (Fig. 1b). This is much smaller than the standard deviation of the average sea surface temperature over the central and eastern tropical Pacific (here defined as 170W-90W, 3S-3N), which is about 1.6 °C. That is, the temporal range of the 40-yr mean Niño-3b SSTs is small compared to the overall spatial variance. This raises the question of whether such small changes in temperature really drive such large variability in variance. Since there is not a strong relationship between the average and variance of the 40-year Niño-3b SSTs (Fig. 1b), we can conclude that the mean temperatures are not a good predictor of the changes in variance. Another possibility is that these changes in variance are the result of a change in the shape of ENSO, which has implication for teleconnections like those shown by Kumar et al. (2006). However, there is not much of a difference in the shape of ENSO between the high and low variance 40-year epochs in the CM2.1 control run (Fig. 2).

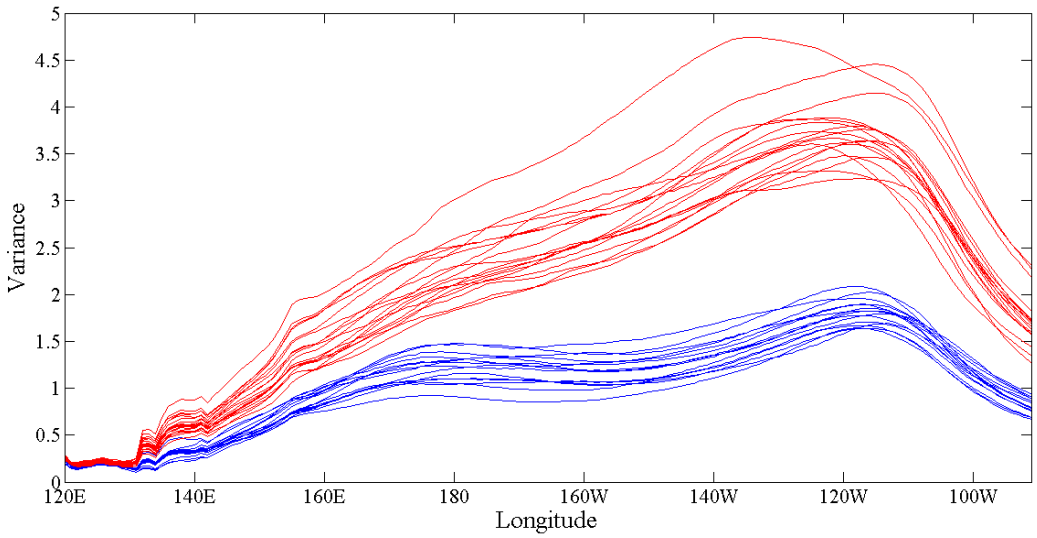

Figure 2. Variance of SST anomaly, averaged over 3S–3N, during high (red) and low (blue) variance 40-yr periods (i.e. the epochs above and below the dashed lines in Figure 1a).

Given that these simple mechanisms seem unconvincing, we use the linear regression of SST changes put forth by van Oldenborgh et al. (2005), where we consider the relative sizes of the three regression coefficients to represent the strength of the ocean-atmosphere coupling. If this coupling is not constant over different time periods, it would imply that the coupling is not random and that there may be a mechanism driving the changes in coupling strength with time. This makes it possible to extend the Wittenberg (2009) results to evaluate the strength of long term changes in ENSO amplitude and investigate potential mechanisms for the variation.

2. Theory and Methodology

Several mechanisms play a role in the fluctuations associated with ENSO in this region: coastal and equatorial upwelling, the zonal SST gradient, east-west sea level pressure asymmetry, the depth of the thermocline, and atmospheric circulation over the equator. These various components determine the characteristics of ENSO. In essence, there is a positive feedback loop whereby anomalously warm SSTs produce a zonal pressure asymmetry, which

produces westerly wind anomalies over the equator; these anomalous winds cause wave propagation in the top layers of the ocean which force the thermocline to deepen in the west and shoal in the east (Fig. 3). Conversely easterly anomalies result in coastal upwelling which brings cooler deep seawater up to the surface of the eastern equatorial Pacific, thereby increasing the zonal SST gradient. The inner loop in Figure 3 portrays how the zonal winds push the cooler upwelled waters in the east toward the west, thereby cooling the ocean surface.

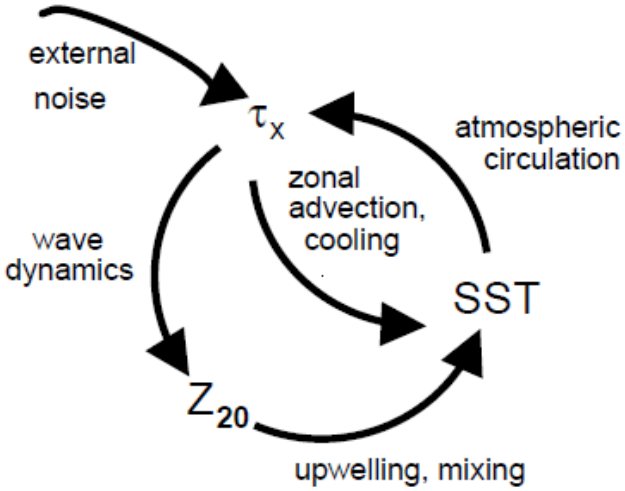

Figure 3. The main feedbacks in the ENSO cycle (van Oldenborgh et al. 2005) – licensed under a Creative Commons License 2.0.

The relative strengths of these processes in forcing SST anomalies can be modeled using a linear regression. Van Oldenborgh et al. (2005) have shown that changes in SST anomalies in the central and eastern Pacific can be well simulated by a linear function of thermocline depth, zonal wind stress and local SST. Such a linear function is motivated by the linearized perturbation advection equation for an incompressible flow in two dimensions Eq. (1), assuming no meridional motion.

$$\frac{\partial T'}{\partial t} + \overline{u}T'_x + \overline{w}T'_z + u'\overline{T}_x + w'\overline{T}_z = Q' \qquad (1)$$

T indicates the temperature and the subscripts indicate a derivative with respect to either the zonal (*x*) or vertical (*z*) direction. Over-bars and primes indicate mean and perturbation quantities respectively. The zonal and vertical velocities are denoted by *u* and *w* respectively. The first term of Eq. (1) is the change in SST anomalies with time. The second and third terms account for the combined effects of the perturbation temperature gradient and the mean velocity field. The vertical perturbations and mean flow dominate this process and are to first order dependent on the upwelling and mixing of thermocline depth anomalies. Therefore, it is reasonable to hypothesize that these two terms can be represented as a linear function of the thermocline depth anomaly. The fourth and fifth terms represent how the perturbation velocity field influences the mean temperature gradients. This term is expected to be linearly related to the zonal wind stress. The final term *Q'* is the perturbation heat flux from the atmosphere to the ocean, including the feedback of SSTs on air-sea fluxes, which can be approximated by a linear relaxation of the temperature anomalies. As a result, Eq. (1) can be simplified into a linear regression equation Eq. (2) where the changes in SST with time are regressed onto Z_{20} (the depth of the 20°C isotherm), τ_x (the zonal wind stress) and the local SST. The resulting weights/coefficients on each of the linear terms provide a first order estimate of the strength of atmosphere-ocean coupling. This simplification allows for the quantification of the complex processes involved in ENSO.

$$\frac{\partial SST}{\partial t}(x,y,t) = \alpha(x,y)\cdot Z_{20}(x,y,t-\delta) + \beta(x,y)\cdot \tau_x(x,y,t) - \gamma(x,y)\cdot SST(x,y,t) \qquad (2)$$

where $$\frac{\partial SST}{\partial t}(x,y,t) = SST(x,y,t+1) - SST(x,y,t)$$

The parameters α and β determine the influence of the thermocline depth anomalies and zonal wind stress anomalies respectively on the change in SST anomalies. The time *t* indicates the time step in months; *x* and *y* indicate the zonal and meridional indices respectively. The parameter γ is a damping coefficient for the SST anomalies. Thermocline depth anomalies are lagged by a factor δ, which represents the finite upwelling time, because thermocline depth anomalies tend to lead SST anomalies with a delay ranging from 2 weeks in the eastern Pacific to 1 year in the central Pacific (Zelle et al. 2004). Although the finite upwelling time δ varies zonally, fitting a zonally variable δ produces unstable results; sharp changes in δ (e.g. from one month to two months) are associated with sharp changes in the other parameters from one time period to another. Such correlated changes in parameters are characteristic of a model which is over-fit, suggesting that zonal wind stress and lagged thermocline depth anomalies are not independent. Thus, in contrast to van Oldenborgh et al. (2005) we chose to keep δ constant at 1 month. Following the methodology of van Oldenborgh et al. (2005), the parameters are computed as functions of both latitude and longitude and then they are averaged over 3S – 3N. Each of the variables (SST, Z_{20} and τ_x) is first reduced to monthly anomalies.

Van Oldenborgh et al. (2005) evaluated the performance of Eq. (2) on climate models which were prepared for the Intergovernmental Panel on Climate Change (IPCC) Fourth Assessment Report (4AR) and on observations from the Tropical Atmosphere Ocean (TAO) array. The models exhibit varying sensitivities to the feedback processes captured by the parameters in the regression. Of all the models tested, the GFDL-CM2.1 model (20^{th} century run) is among the top performers in exhibiting a realistic and balanced ENSO cycle as depicted by the parameter strengths when compared to observations (Van Oldenborgh et al. 2005). However, the GFDL-CM2.1 20^{th} century runs have climate-forcing built in. Therefore, one may

wonder how Eq. (2) would perform on a model where there is no climate forcing built in? Therefore, this paper examines the performance of the Van Oldenborgh et al. (2005) linear regression method on the GFDL-CM2.1 4000-yr control run.

The 4000-yr pre-industrial control run of the GFDL CM2.1 model couples atmosphere, ocean, land, and sea ice components (Delworth et al. 2006). The atmospheric component has a horizontal resolution of 2.5° longitude by 2.0° latitude, with 24 vertical levels. The ocean component has a horizontal resolution of 1° in the extratropics, with zonal spacing reducing to 1/3° near the Equator. The model has 50 vertical levels, the first 22 of which are evenly spaced by 10 meters. The CM2.1 model is ranked among the world's best GCMs in terms of its simulation of global climate as well as ENSO [van Oldenborgh et al., 2005; Wittenberg et al., 2006; Guilyardi, 2006; Reichler and Kim, 2008]. The model does not use flux adjustments. The control run holds atmospheric composition, insolation and land cover constant at 1860 values, which means that all variability in the simulation is internally produced, as opposed to having any anthropogenic climate forcings. Finally, the length of the 4000-yr simulation makes it a prime subject to analyze long-term climate variability.

The GFDL ensemble coupled data assimilation (ECDA) system is based on the fully coupled climate model CM2.1. The use of ensemble assimilation means that the CM2.1 model is used to interpolate in data-poor regions and time periods. Because the model is essentially the same as that used in free-running mode any differences are likely due to the addition of data constraints, rather than to some underlying difference in physical parameterizations. This study uses ECDA reanalyzed ocean temperatures and surface wind stresses for the period 1960-2010 (Zhang et al. 2007) in order to understand the natural variability of the tropical Pacific. The ECDA has been

shown to be a good representation of the ocean variability associated with ENSO and other climate modes (Chang et al. 2012).

3. Results

The resulting averaged regression coefficients from Eq. (2) are shown in Figure 4. The effects of the ENSO positive feedback loop are manifested in the regional strengths of each of the parameters. These plots indicate how the temperatures near the equator are forced by thermocline depth and zonal wind stress and how they are damped. The parameters are evaluated on 40-yr time periods in order to understand how they change on multi-decadal time scales. On longer evaluation periods, such as 500 years (no shown), the regression coefficients are more well-constrained across epochs. On the other hand, shorter evaluation periods, such as 40 years, produce widely ranging parameter amplitudes across epochs. These multidecadal regression coefficients range within about a factor of 2 from the 4000-yr regressed amplitude. The regression coefficients, and therefore the ocean-atmosphere coupling strengths, are not constant in the control run but in fact change on decadal to multicentennial scales.

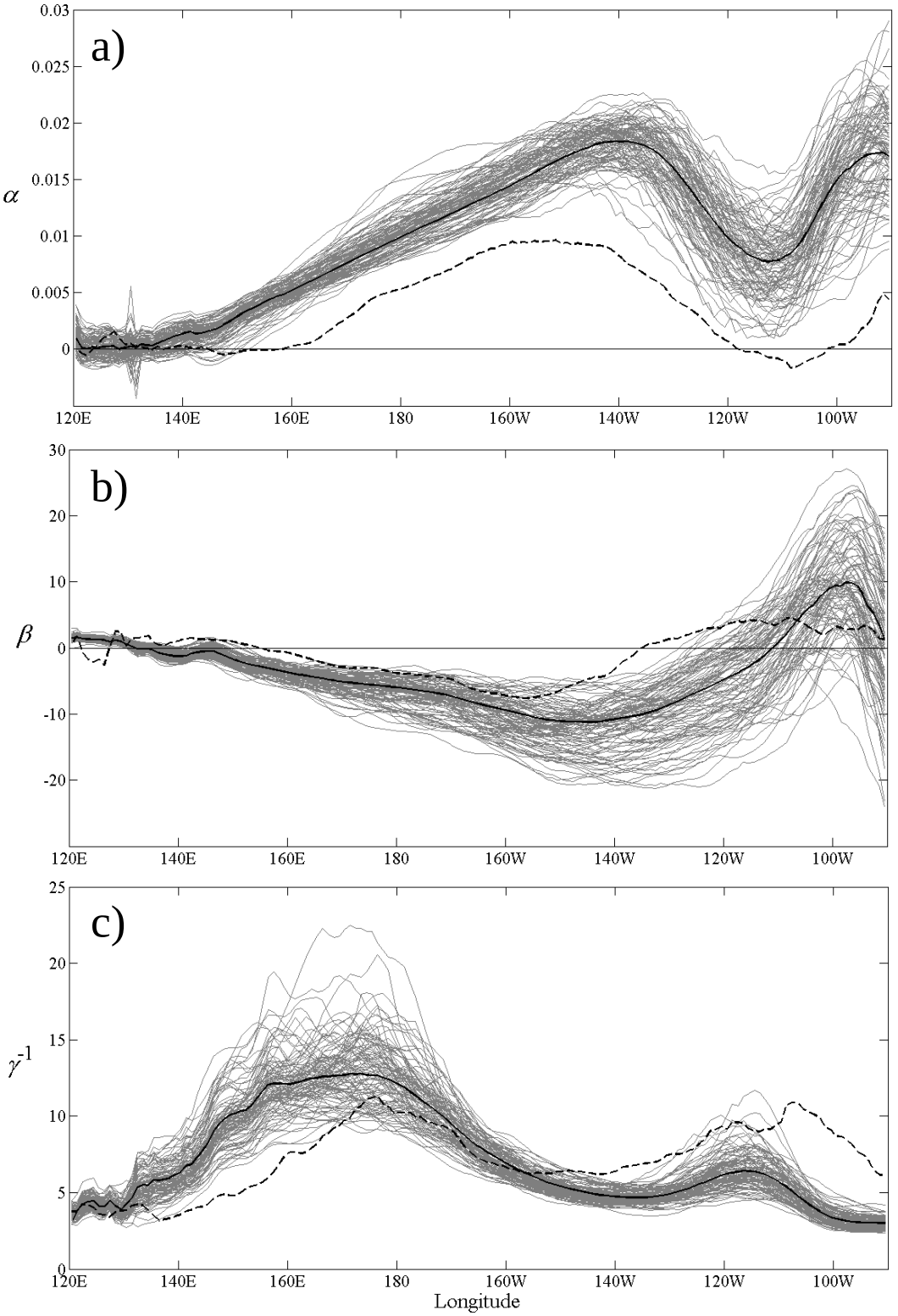

Figure 4. Regression coefficients (a) α (km^{-1} month^{-1}) – thermocline depth parameter, (b) β (kPa^{-1} month^{-1}) – the wind stress parameter and (c) γ^{-1} (months) – the damping time – averaged over 3S–3N in the CM2.1 4000-yr control run (bold black), 40-yr epochs of the CM2.1 control run (gray) and the ECDA reanalysis data (dashed bold black). A black line is plotted for easy identification of the zero line.

These regression coefficients are not directly comparable to those calculated by the original study of van Oldenborgh et al. (2005) from the climate-forced GFDL CM2.1 simulation and from observations for three reasons: the use of variable or constant finite upwelling time, climate forcings, and evaluation time scales. This study uses a constant finite upwelling time as opposed to a variable one. The GFDL CM2.1 20th century run has climate-forcings built in, while the 4000-yr control run keeps climate parameters constant at 1860 values. Van Oldenborgh et al. (2005) evaluated a single century, while we evaluate multiple centuries, in addition to other time scales. From our analysis, we can infer that a single century regression may produce regression coefficients that differ significantly in amplitude from other centuries.

Comparing the regression coefficients presented in this study to the observationally-derived regression coefficients in van Oldenborgh et al.'s (2005) paper is also complicated because it would be difficult to determine what amount of the differences are due to model inadequacies in representing the real-world, and what amount is due to the difference of including or excluding climate-forcing. In an effort to address this issue, the regression is performed on the GFDL ECDA reanalysis, which has been shown to agree well with observations in both climatology and variability for the 51 year period between 1960 and 2010. The resulting averaged regression coefficients, shown in Figure 4 as the bold dashed black lines, show qualitative agreement with the CM2.1-regressed coefficients, shown in Figure 4 as the bold solid black lines, except for β. Some of these discrepancies may be due to the following assumptions made during the regression of ECDA values: the thermocline depth is calculated as the depth of the 20°C isotherm based on a linear relationship between the two closest temperatures; if the first temp at 5m depth is already below 20°C, the thermocline depth is set to 2.5m. That the coupling

coefficients are stronger and the damping weaker may help explain why the CM2.1 model has an overly vigorous ENSO.

4. Mechanisms

As expected, the varying strength of the ocean-atmosphere coupling on decadal to multicentennial scales is related to ENSO variability. Figure 5 shows the correlation between the regression coefficients and the Niño-3b SST variance for each 40-yr epoch as a function of longitude. The dashed lines draw the eye to the regions that exhibit correlations above 0.5 and below -0.5. The γ parameter is not significantly correlated with Niño-3b variance except in the eastern equatorial Pacific where there is a strongly negative correlation. This is not unexpected because a higher relaxation time would generally lead to a damping of the ocean-atmosphere coupling and therefore lower Niño-3b variance. The β wind stress parameter is highly correlated with the Niño-3b SST variance on 40-yr time scales through most of the central and eastern equatorial Pacific basin. The α parameter on the other hand has a negative correlation with Niño-3b variance within about 10° of 180°W and a positive correlation around 130°W.

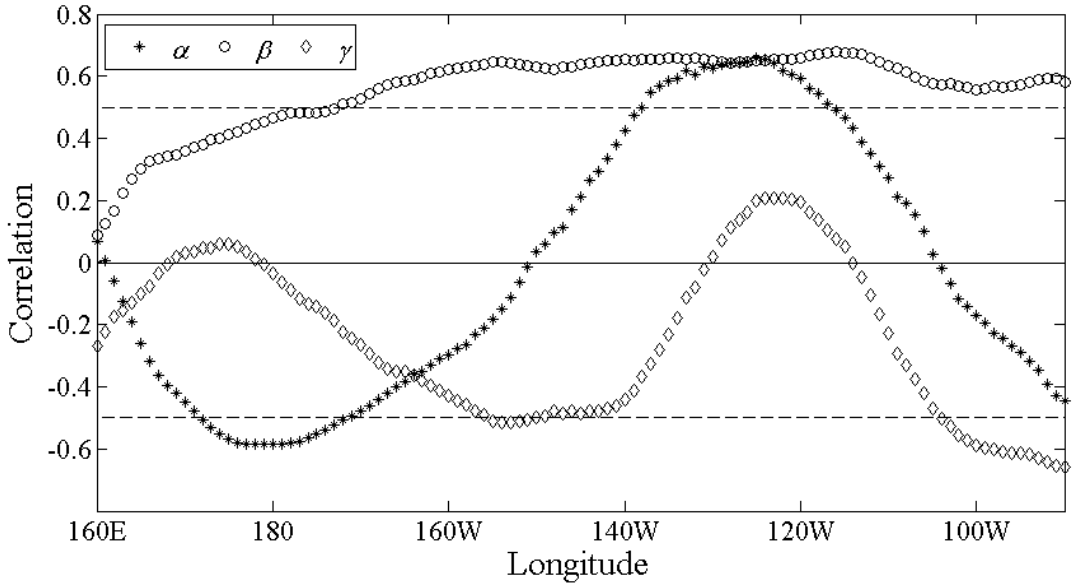

Figure 5. Correlation between the average regression coefficients and the Niño-3b SST variance on 40-year time periods. Dashed black lines draw attention to the 0.5 correlation coefficient level.

Returning to the advection equation on which the regression is based may help to determine what forces are driving SST variability. As we stated earlier, the β parameter is expected to represent $\bar{u}'\nabla\overline{T}$ – how the perturbation velocity field advects the mean temperature gradient. Since there is a high correlation between the β parameter and Niño-3b variance in the equatorial Pacific, this suggests that a large source of the variability in SSTs may be due to the changes in the background temperature gradient. Therefore, we hypothesize that the changes in the strength of the ocean-atmosphere coupling, as manifested by the regression coefficients on multi-decadal time scales, are driven in large part by changes in temperature stratification in the mid-Pacific. The temperature stratification of subsurface equatorial ocean water is highly correlated with the Niño-3b SST variance on multi-decadal timescales in the mid-Pacific at depths of about 50-100 m (Fig. 6). That is, the temperature stratification increases in the upper 100 m of the mid-Pacific equatorial waters when there is higher Niño-3b SST variance. This increased stratification in the mid-Pacific represents a shoaling of the thermocline, while the decreased stratification in the eastern Pacific represents a deepening of the thermocline. This shows that coupling strength is

indeed related to stratification in the mid-Pacific as hypothesized. In fact, as the ENSO amplitude changes by a factor of two, so does the mid-Pacific stratification on 40-yr time periods (Fig. 7).

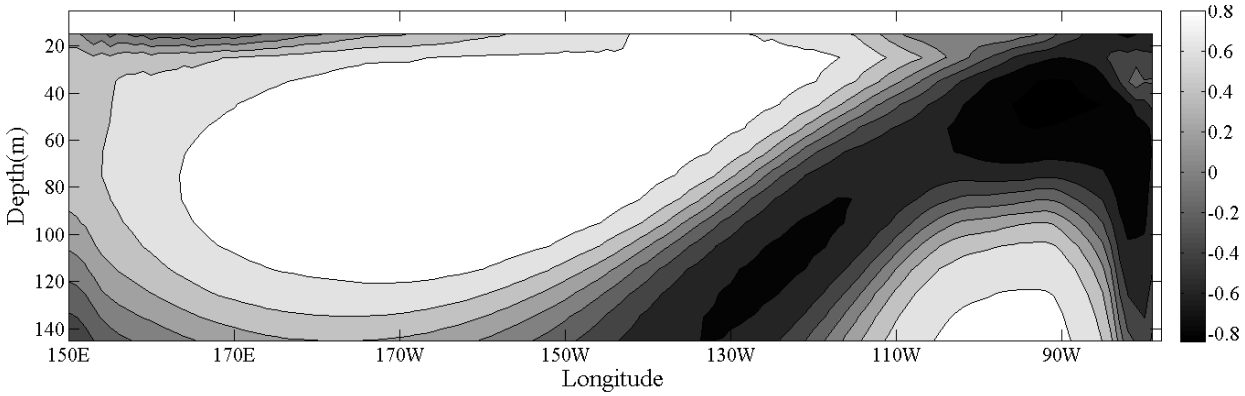

Figure 6. Correlation between the average temperature stratification in the top 60 meters of the ocean averaged from 3S–3N and the 40-yr Niño-3b variance.

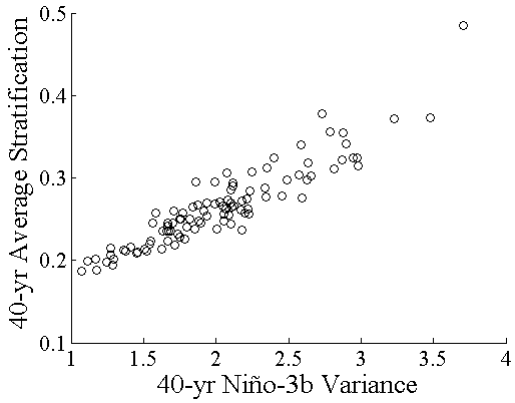

Figure 7. 40-yr average stratification (60 meters to surface) in the region 170E–150W vs. 40-year variance of the Niño-3b SST anomalies.

However, the two-fold changes in ENSO variance are not solely explained by changes in β because there are also strong correlations with α. Looking again at Figure 5, the correlation between α and the Niño-3b variance is less intuitive. There is a negative correlation between 170°E and 170°W and a positive correlation between 138°W and 118°W. In the western basin, shallower thermocline depths produce larger ENSO variance. While in the eastern basin, deeper thermocline depths produce larger ENSO variance. This dual-correlated behavior indicates that decades with flatter thermoclines have stronger Niño-3b variance.

From the advection equation, α would be expected to represent $\bar{\vec{u}}\nabla T'$ – the effects of the perturbation temperature gradient advected by the mean velocity field. Since the most prominent velocities are in the vertical direction, α is expected to represent the impact of $\bar{w}\partial T'/\partial z$ on $\partial T/\partial t$. Therefore, we might expect that the changes in α are due to changes in the mean vertical velocity field, with strong upwelling resulting in a greater sensitivity to Z_{20}. However, in looking at the mean upwelling speeds in the two regions where α exhibits a significant correlation with Niño-3b SST variance, there is an opposite relationship with Niño-3b SST variance. For example, in the region 170E–170W, there is a negative correlation between α and SST variability, but there is a positive correlation between mean upwelling speeds and SST variability and vice versa for the region 118–138W (Fig. 8). Therefore, changes in the mean upwelling cannot be the reason for changes in the variance.

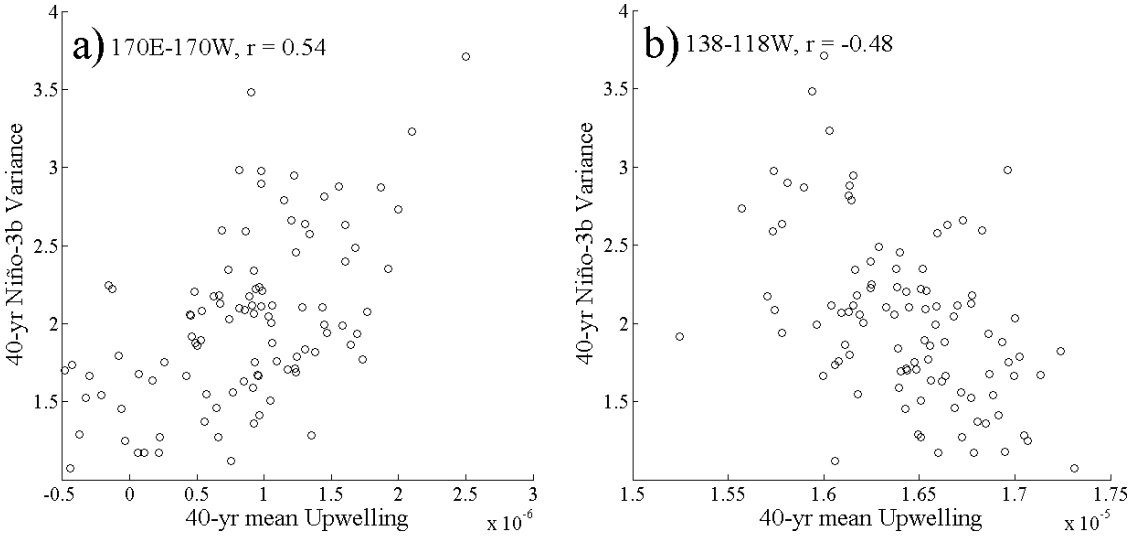

Figure 8. 40-year Niño-3b variance vs. 40-year mean upwelling (a) 170E–170W (a region where α is anticorrelated with variance) and (b) 138–118W (a region where α is positively correlated with variance).

Additionally, the influence of Z_{20} on SST is not necessarily the source of the change in the correlation with Niño-3b variance. In the region 170E-170W, where α has a highly negative correlation with Niño-3b variance, there is a distinguishable difference between the regression

coefficient of SST onto Z_{20} in times of high and low Niño-3b variance (Fig 9a), but it is the opposite relationship. In the region 138-118W, where α has a highly positive correlation with Niño-3b variance, there is not a distinguishable difference between the regression coefficient of SST onto Z_{20} in times of high and low Niño-3b variance. This implies that the correlation between Z_{20} and SST is secondary to a more dominant source of variability. In order to determine what drives the changes in α, we look more carefully at the ENSO feedback cycle (Fig. 3) in search of an indirect effect.

Due to the nature of the regression, α may be capturing another part of the feedback cycle. In the regression of τ_x onto SST (Fig. 9b), where there is some distinguishability between the high and low variance periods in the two regions of high correlation between α and Niño-3b variance in Figure 6. In effect, α is capturing the portion of the ENSO cycle where SST feeds back onto τ_x. This pathway cannot be captured by β because the regression inherently fixes the zonal winds when determining β. In essence, by making the assumptions outlined in the theory and methods sections, the α term picks up the lagged effect of the temperature on itself – the indirect effect of the previous SST on the current SST – as mediated by the wind stress.

In addition, there is a stronger response of τ_x to anomalous temperatures over the central Pacific during times of higher variance than during times of lower variance (Fig. 9b). This supports the idea proposed by Anderson et al. (2009) that a warming of the eastern Pacific results in an increase in ENSO amplitude. Accordingly, the periods when Z_{20} is shallower in the west and deeper in the east correspond to times when the temperatures in the east (west) are warmer (cooler) and thus to times when the wind stress is more (less) responsive. That is, during high variance periods, the wind stress anomalies penetrate more into the central part of the basin

where the magnitude of β is larger. This indirect process produces much of the correlation between the large-scale temperature structure and the variance.

Furthermore, there is a much stronger response of τ_x to anomalous temperatures during El Niño than during La Niña throughout most of the central and eastern equatorial Pacific, as shown by the interannual regression between the wind stress anomalies and SST anomalies during the different phases of ENSO (Fig. 10). Therefore, it seems that much of the variability in the alpha coefficient is dominated by El Niño periods.

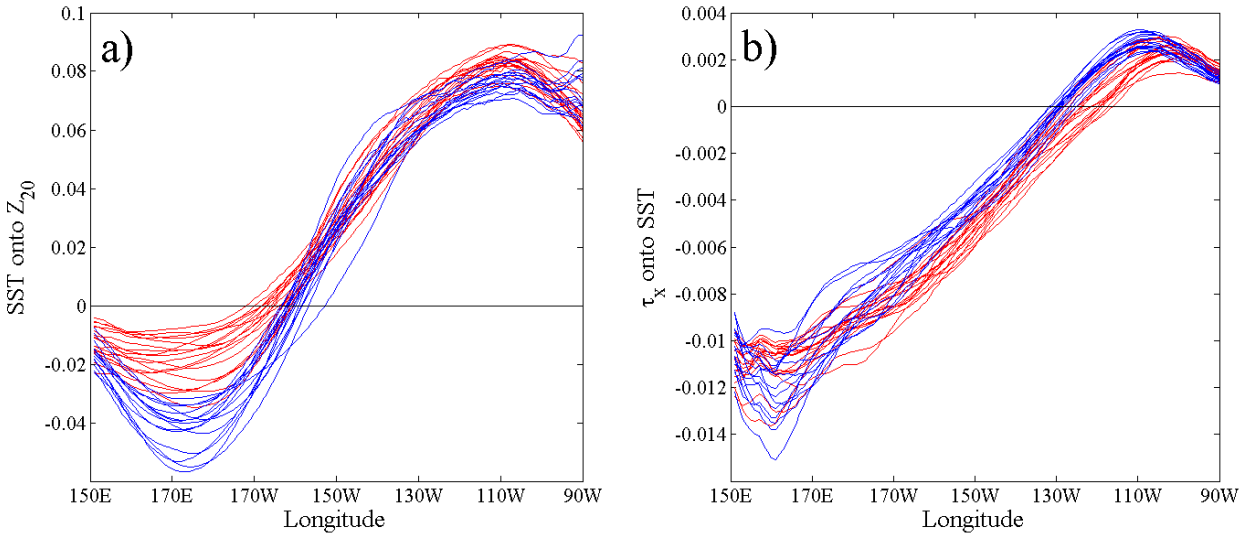

Figure 9. Regression coefficients averaged over 3S–3N for (a) SST regressed onto Z_{20} and (b) τ_x regressed onto SST in times of high (red) and low (blue) Niño-3b variance 40-yr periods.

5. Discussion and Conclusions

ENSO is a dynamic process which exhibits variability over a range of different timescales (Wittenberg, 2009). We use the linear regression technique from van Oldenborgh et al. (2005), to examine the causes of multidecadal variability in Niño-3b variance found in the GFDL CM2.1 coupled model. When applied to the ECDA reanalysis data (performed using the same basic model configuration but strongly constrained by observations) the regression produces

coefficients with similar structures as those produced by the model. However, the regression coefficient between wind stress and SST change is larger in the model than in the data, as is the damping time for SST anomalies. These results may explain why the CM2.1 model produces an overly vigorous ENSO than has been seen over the past 50 years.

Applying the analysis to the long-term modulation of ENSO, we find changes in the coupling between the ocean and the atmosphere about a factor of two on multi-decadal time scales. Changes in the regression coefficient between wind stress and temperature change have a clear signature in ocean stratification, with periods of high stratification associated with stronger coupling. Changes in the regression coefficient between thermocline depth and temperature change appear to reflect the mean state of the atmosphere and its sensitivity to tropical temperature variability (as in Anderson et al. 2009) rather than directly reflecting changes in advective heating and cooling. Understanding such signatures of ENSO variability may contribute to the predictability of El Niño.

These results have implications for evaluating and improving climate models. They suggest that it requires not only multiple decades to centuries of model runs to characterize the natural ENSO variability (Stevenson et al. 2012), but to constrain the internal coupling strengths as well. One needs to be careful using only 40 years of data to constrain model physics. This highlights the importance of producing longer proxy records of tropical temperature variability, so that we can evaluate whether the mechanisms proposed here actually work in the real world. Furthermore, the results seem to suggest that when the CM2.1 model has a weaker (putatively more realistic) cold tongue, it ends up with a stronger (putatively less realistic) El Niño. While this result is unlikely to be true for all coupled models, it nonetheless shows how important it is to constrain all parts of the coupling cycle. Simply reducing the mean bias in one part of the

system will not necessarily produce a more realistic model overall. In summary, this paper confirms previous studies on the long-term variability of ENSO, while extending these results by identifying the driving mechanism as due to changes in coupling and identifying the signature of these changes in the long-term mean state of the ocean and atmosphere.

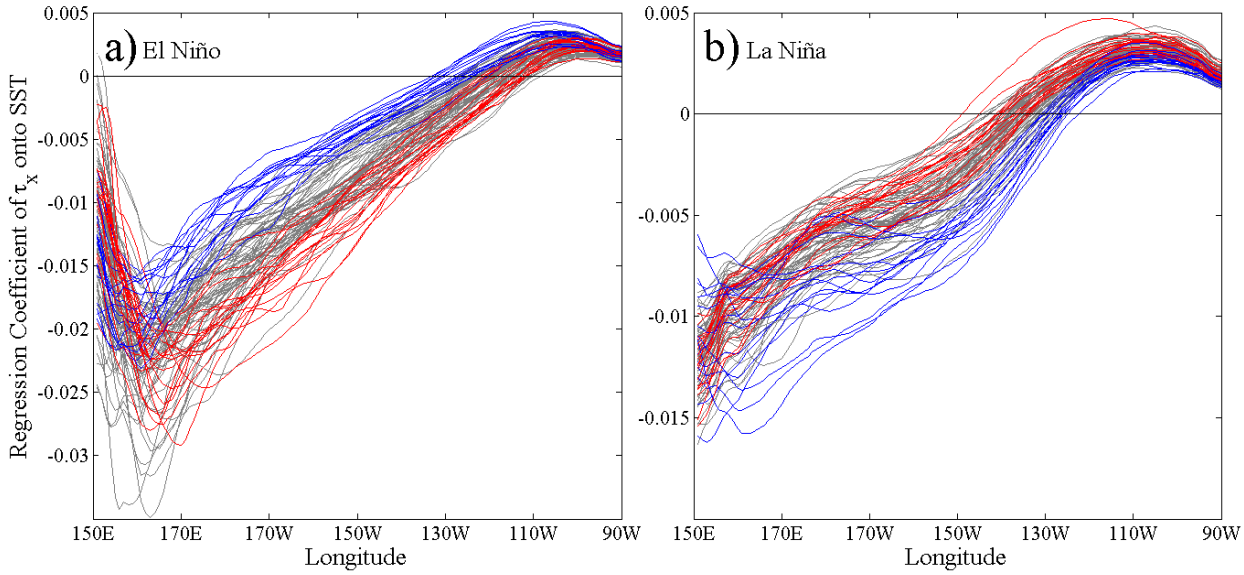

Figure 10. Regression coefficient of τ_x onto SST (averaged over 3S–3N) for every 40-year epoch during (a) El Niño months and (b) La Niña months, stratified by 40-yr Niño-3b variance: high variance (red) and low variance (blue) periods.

Our analysis makes the assumption that a linear regression is sufficient to understand these processes. This is supported by the fact that when we use variable finite upwelling delays, the regression model is in danger of over-fitting the data. However, when we look at the interannual regression between the wind stress anomalies and SST anomalies during the different phases of ENSO, some interesting patterns emerge that suggest the picture may not be so simple (Fig. 10). Not only is there a separation in the regression pattern between El Niño and La Niña periods, but there is a strong difference in the behavior of high variance 40-year epochs for different ENSO phases. This gives an indication of nonlinearity coupling.

Acknowledgements. The authors gratefully acknowledge NOAA's Geophysical Fluid Dynamics Laboratory's provision of both the CM2.1 model and Ensemble Coupled Data Assimilation. We thank Andrew Wittenberg for useful discussions. AR acknowledges support from NSF through the Water, Climate and Health IGERT at Johns Hopkins University.

References

Anderson, W., A. Gnanadesikan, and A. Wittenberg, 2009: Regional impacts of ocean color on tropical Pacific variability. *Ocean Sci. Discuss.*, **6**, 243–275.

Burgers, G. and G. J. van Oldenborgh, 2003: On the Impact of Local Feedbacks in the Central Pacific on the ENSO cycle. *J. Climate*, **16**, 2396–2407.

Chang, Y. -S., S. Zhang, A. Rosati, T. L. Delworth, and W. F. Stern, 2012: An assessment of oceanic variability for 1960-2010 from the GFDL ensemble coupled data assimilation. *Clim. Dyn.*, **40**, doi:10.1007/s00382-012-1412-2.

Delworth, T. L., et al., 2006: GFDL's CM2 global coupled climate models. Part I: Formulation and simulation characteristics. *J. Climate*, **19**(5), 643–674.

Dijkstra, H. A. and G. Burgers, 2002: Fluid Dynamics of El Niño Variability. *Annu. Rev. Fluid Mech.*, **34**, 531–558.

Guilyardi E., 2006: El Niño–mean state–seasonal cycle interactions in a multi-model ensemble. *Clim. Dyn.*, **26**, 329–348.

Kumar, K. Krishna, et al., 2006: Unraveling the Mystery of Indian Monsoon Failure During El Niño. *Science*, **314**, 115–119.

Stevenson, S., B. Fox-Kemper, M. Jochum, R. Neale, C. Deser, and G. Meehl, 2012: Will There Be a Significant Change to El Niño in the Twenty-First Century? *J. Climate*, **25**, 2129–2145.

van Oldenborgh, G.J., et al., 2005: El Niño in a Changing Climate. *Ocean Science*, **1**, 81–95.

Wittenberg, A. T., A. Rosati, N.-C. Lau, and J. J. Ploshay, 2006: GFDL's CM2 global coupled climate models. Part III: Tropical Pacific climate and ENSO. *J. Climate*, **19**, 698–722.

Wittenberg, A. T., 2009: Are historical records sufficient to constrain ENSO simulations? *Geophys. Res. Lett.*, **36**, L12702, doi:10.1029/2009GL038710.

Zelle, H., G. Appeldoorn, G. Burgers, and G. J. van Oldenborgh, 2004: The relationship between sea surface temperature and thermocline depth in the eastern equatorial Pacific. *J. Phys. Oceanogr.*, **34**, 643–655.

Zhang S., M.J. Harrison, A. Rosati, and A.T. Wittenberg, 2007: System design and evaluation of coupled ensemble data assimilation for global oceanic climate studies. *Mon. Weather. Rev.*, **135**, 3541–3564.